J Braz. Soc. Mech. Sci. Eng. (2017) 39:4379–4391
DOI 10.1007/s40430-017-0765-1

TECHNICAL PAPER

Magnetohydrodynamic micropolar nanofluid past a permeable stretching/shrinking sheet with Newtonian heating

K. Gangadhar[1] · T. Kannan[2] · P. Jayalakshmi[3]

Received: 26 July 2016 / Accepted: 14 March 2017 / Published online: 28 March 2017

Abstract In this present study, a numerical investigation has been carried out to discuss the steady, two dimensional flow and heat transfer on micropolar nanofluid over a stretching/shrinking sheet with variable suction or injection in the presence of magnetic field and Newtonian heating. Copper (Cu), alumina (Al_2O_3) and titanium (TiO_2) in water-based micropolar nanofluid has been considered for the present investigation. The solutions of the transformed nonlinear equations have been obtained using Runge–Kutta–Gill procedure together with the shooting method. The results are presented graphically and discussed for various resulting parameters. Dual solutions are found to exist in a certain range of the governing parameters. The thickness of thermal boundary layer for Cu nanofluid is more than that of other nanofluids in the cases of shrinking and stretching sheets. Newtonian heating effect significantly increases the thermal boundary layer thickness for both sheets under investigation.

Technical Editor: Jader Barbosa Jr.

✉ T. Kannan
tkannanmat@gmail.com

K. Gangadhar
kgangadharmaths@gmail.com

P. Jayalakshmi
jayachetu85@gmail.com

[1] Department of Mathematics, Acharya Nagarjuna University, Ongole, Andhra Pradesh 523001, India

[2] Department of Mathematics, K. S. Rangasamy College of Technology, Tiruchengode, Tamil Nadu 637215, India

[3] Department of Mathematics, Vemu Institute of Technology, P. Kothakota, Chittoor, Andhra Pradesh 517512, India

Keywords Micropolar nanofluid · MHD · Stretching or shrinking · Suction or injection · Newtonian heating

List of symbols

B_0	Magnetic induction (T)
c	Constant defined by Eq. (2.8)
C_f	Skin friction coefficient
C_n	Wall couple stress
c_p	Specific heat at constant pressure (J/kg K)
f	Dimensionless stream function
f_w	Suction/injection parameter
g	Dimensionless micro rotation
h	Convective heat transfer coefficient
j	Microinertia density
K	Micropolar or material parameter
k	Thermal conductivity (W/mK)
M	Magnetic parameter
n	Constant defined by Eq. (2.5)
N	Microrotation component
Nu_x	Local Nusselt number
Pr	Prandtl number
q_w	Surface heat flux (W/m^2)
Re_x	Local Reynolds number
T	Temperature of the fluid (°C)
u_w	Stretching velocity
u, v	Velocity components (m/s)
v_w	Mass transfer velocity
x, y	Dimensionless coordinates

Greek symbols

α	Thermal diffusivity (m^2/s)
γ	Conjugate parameter for Newtonian heating
δ	Spin-gradient viscosity
η	Similarity variable
θ	Dimensionless temperature

κ Vortex viscosity
λ Stretching/shrinking parameter
μ Thermal viscosity (kg s/m)
υ Kinematic viscosity (m^2/s)
ρ Density (kg/m^3)
σ Electrical conductivity (s/m)
τ_w Wall shear stress
ϕ Nanoparticle volume fraction
ψ Stream function (m^2/s)

Subscript
f Base fluid
nf Nanofluid
s Solid
w Condition at the surface
∞ Condition at infinity

Superscript
$'$ Differentiation with respect to η

1 Introduction

Nanofluids are suspensions of nano-sized particles in common fluids that show significant enhancement of their properties at modest nanoparticle concentrations. Most generally used nanoparticles are aluminum, copper, iron and titanium or their oxides. Consideration of nanofluids in a variety of processes results in noteworthy applications in engineering and sciences since materials with sizes of nanometers possesses unique physical and chemical properties. Several investigations in literature reveals the fact that nanofluids have been found to have enhanced thermophysical properties such as thermal conductivity, thermal diffusivity, viscosity and convective heat transfer coefficients compared to those of base fluids like oil or water. Choi [8] is the first who introduced the term nanofluids to refer to the fluid with suspended nanoparticles. Choi et al. [9] reported that the addition of a small amount of nanoparticles to conventional heat transfer liquids notably increases the thermal conductivity of the fluid up to approximately two times. Buongiorno [6] concluded that only Brownian diffusion and thermophoresis are essential slip mechanisms in nanofluids. Makinde and Aziz [24] examined the flow of a nanofluid past a stretching sheet with a convective boundary condition and found that as the Prandtl number increases, the thickness of the thermal boundary layer decreases as the curves become increasingly steeper. Makinde and Mishra [25] studied the stagnation point flow of variable viscosity nanofluids past a stretching surface with radiative heat.

The study of fluids with micro-structures has acquired a great attention due to its significant role playing in industrial and engineering applications. Micropolar fluids are fluids with micro-structure. They belong to a class of fluids with non-symmetric stress tensor that shall call polar fluids and include as a special case, the well-constructed Nevier–Stokes model of classical fluids that we shall call ordinary fluids. Physically, micropolar fluids may represent fluids consisting of rigid, randomly oriented (or spherical) particles suspended in a viscous medium, where the deformation of fluid particles is ignored. The theory of micropolar fluids were introduced by Erignen [13, 14]. Arafa and Gorla [2] carried out a work on the buoyancy and curvature on convection of micropolar fluid along vertical cylinders and needles. It is concluded that non-homogeneous boundary conditions for microrotation significantly enhance the microrotation. Nadeem et al. [29] investigated the stagnation point flow of a micropolar nanofluid in a moving cylinder with finite radius. It is confirmed that the velocity, angular velocity and temperature at the surface increased by increasing micropolar parameter value. Bourantas and Loukopoulos [4] presented an analysis of natural convection of a micropolar nanofluid (Al_2O_3/water) along inclined rectangular enclosure. Noor et al. [32] discussed the mixed convection flow of a micropolar nanofluid near a stagnation point past a vertical stretching sheet. It is found that the flow becomes cooler and the nanoparticle volume fraction is reduced with an increase in Prandtl number. Rehman and Nadeem [39] reported the applicability of boundary layer theory for the mixed convection flow of micropolar nanofluid on a vertical slender cylinder. It was illustrated that the velocity and temperature of the fluid at the boundary is decreased as the micropolar parameter increased. Ram Reddy et al. [37] examined the similarity solution for the steady free convection flow of a micropolar fluid past a vertical plate with convective boundary condition. They proved that microrotation, temperature, and concentration distributions and skin friction coefficients are more in the case of a micropolar fluid with strong concentration when compared to the case of a micropolar fluid with weak concentration.

Magnetohydrodynamic (MHD) boundary layers with heat and mass transfer over flat surfaces are found in many engineering and geophysical applications such as geothermal reservoirs, thermal insulation, enhanced oil recovery, packed-bed catalytic reactors, and cooling of nuclear reactors. Many chemical engineering processes like metallurgical and polymer extrusion processes involve cooling of a molten liquid being stretched into a cooling system. The fluid mechanical properties of the penultimate product depend mainly on the cooling liquid used and the rate of stretching. Some polymer liquids like polyethylene oxide and polyisobutylene solution in cetane, having better electromagnetic properties are normally used as cooling liquid as their flow can be regulated by external magnetic fields

to improve the quality of the final product. Jat and Jhankal [19] concluded that the skin friction coefficient increases with increasing the values of Reynolds number and magnetic parameter up to a certain value of Reynolds number and afterwards it decreases with the increasing values of these parameters and also the heat transfer rate increases with increasing the values of these parameters. Hayat and Nawaz [18] studied the effects of MHD on three dimensional flow of a second grade fluid with heat transfer and they concluded that dimensionless tangential velocity is a decreasing function of magnetic field, whereas dimensionless lateral velocity increases by increasing magnetic parameter. Turkyilmazoglu [42] analyzed the three dimensional MHD laminar stagnation point flow of an electrically conducting fluid in the presence of a uniform vertical magnetic field. It is observed that the stagnation velocities and shear stresses are strongly dependent upon the magnetic field parameter. Hayat et al. [17] reported that the three dimensional flow of MHD Eyring–Power fluid with radiation effect and then concluded that magnetic field causes a decrease in the magnitude of velocity components. Kar et al. [21] investigated the effects of MHD, heat source and chemical reaction in a vertical channel through a porous medium and reported that the presence of heavier species contributes to surface mass transfer significantly. Rajagopal et al. [35] examined MHD flow due to impulsive motion with heat and mass transfer past a stretching sheet in a saturated porous medium. It is reported that the magnetic parameter affects significantly the surface shear stress and surface mass transfer. El-Dabe et al. [12] proved that the velocity distribution decreases with increasing the values of magnetic parameter while it increases the values of Casson fluid parameter. Ramzan [38] discussed the influence of Newtonian heating, viscous dissipation and joule heating on the magnetohydrodynamic (MHD) three dimensional couple stress nanofluid past a stretching surface. It is found that velocity components decrease with an increase in couple stress parameter. Gireesha et al. [16] investigated the MHD boundary layer three dimensional flow and heat transfer towards a linearly stretching sheet in the presence of nanoparticle. Das and Jana [11] considered the natural convective magneto-nanofluid flow and radiative heat transfer past a moving vertical plate. It is concluded that the rate of heat transfer at the plate is found to be higher for Cu–water nanofluid. Baag and Mishra [3] investigated the impact of heat and mass transfer analysis on MHD water-based nanofluid and they found that boundary layer thickness reduces in the presence of magnetic field.

The study of stretched flows with heat transfer is given much importance. The heat transfer is through constant wall temperature or constant wall heat flux. Also there are another class of flow problems in which the rate of heat transfer is proportional to the local surface temperature from the boundary surface with finite heat capacity known as Newtonian heating or conjugate convective flow. The boundary layer natural convective flow with Newtonian heating is reported by Merkin [27]. Chaudhary and Jain [7] obtained the similarity solution for unsteady free convection flow past on impulsive vertical surface in the presence of Newtonian heating. It is reported that the increase in the Grashof number, the contribution from the buoyancy near the plate becomes significant. Mohamed et al. [28] concluded that when the value of the conjugate parameter γ decreases it is found that the temperature also decreases. Khan et al. [22] explicated the effects of Newtonian heating and mass diffusion on MHD free convection flow over vertical plate with shear stress at the wall.

The above cited articles in the literature explicates the flow and the heat transfer characteristics of different working fluids in permeable stretching/shrinking sheet with or without variable suction or injection in detail. Obviously, presence or absence of magnetic field and Newtonian heating becomes significant in many research works as explained above. It can be noticed that consideration of copper (Cu), alumina (Al_2O_3) and titania (TiO_2) in water-based micropolar nanofluid as working fluid in the place of base fluids is of greater interest in practical applications in science and engineering. It is found that the solutions of the transformed ordinary differential equations have dual solutions in a certain range of the governing parameters. As a trial attempt, the authors intend to provide the knowledge of the effects of the steady, two dimensional flow of heat transfer on micropolar nanofluid with variable suction or injection in the presence of magnetic field and Newtonian heating.

2 Mathematical formulation

Consider the steady two-dimensional boundary layer flow over a permeable stretching/shrinking sheet in an electrically conducting water-based micropolar nanofluid containing different types of nanoparticles: copper (Cu), alumina (Al_2O_3) and titanium dioxide (TiO_2). The micropolar nanofluid is assumed as incompressible laminar flow. It is also presumed that the base fluid (i.e., water) and the nanoparticles are in thermal equilibrium and no slip occurs between them in quiescent micropolar nanofluid. The thermo-physical properties of the nanofluid are specified in Table 1.

The sheet stretching velocity is $u_w(x) = \lambda x$, where λ is a constant with $\lambda > 0$ corresponds to a stretching sheet. The wall mass transfer velocity is $v_w(x) = v_0$, with $v_0 < 0$ for suction. The x-axis is measured along the stretching surface in the direction of the motion and the y-axis is perpendicular to it. A uniform transverse magnetic field of strength B_0

Table 1 Thermo-physical properties of water and nanoparticles [33]

Physical properties	Water/base fluid	Cu	Al_2O_3	TiO_2
ρ (kg/m^3)	997.1	8933	3970	4250
c_p (J/kg K)	4179	385	765	686.2
k (w/m K)	0.613	401	40	8.9538
ϕ	0.0	0.05	0.15	0.2
σ (S/m)	5.5×10^{-6}	59.6×10^{6}	35×10^{6}	2.6×10^{6}

is applied parallel to the y-axis. It is assumed that induced magnetic field produced by the fluid motion is negligible in comparison with the applied one so that we consider the magnetic field as $\vec{B} = (0, 0, B_0)$. This assumption is justified, since the magnetic Reynolds number is very small for metallic liquids and partially ionized fluids [10]. Also, no external electric field is applied such that the effect of polarization of fluid is negligible [10], so we assume $\vec{E} = (0, 0, 0)$. Schematic diagram of the physical model is shown in Fig. 1.

Under the above assumptions, the governing equations of continuity, momentum, angular momentum, and energy are written as follows:

$$\frac{\partial u}{\partial x} + \frac{\partial v}{\partial y} = 0, \tag{2.1}$$

$$u\frac{\partial u}{\partial x} + v\frac{\partial u}{\partial y} = \frac{\mu_{\rm nf} + \kappa}{\rho_{\rm nf}}\frac{\partial^2 u}{\partial y^2} + \frac{\kappa}{\rho_{\rm nf}}\frac{\partial N}{\partial y} - \frac{\sigma_{\rm nf} B_0^2}{\rho_{\rm nf}}u, \tag{2.2}$$

$$\rho_{\rm nf} j\left(u\frac{\partial N}{\partial x} + v\frac{\partial N}{\partial y}\right) = \delta_{\rm nf}\frac{\partial^2 N}{\partial y^2} - \kappa\left(2N + \frac{\partial u}{\partial y}\right), \tag{2.3}$$

$$u\frac{\partial T}{\partial x} + v\frac{\partial T}{\partial y} = \alpha_{\rm nf}\frac{\partial^2 T}{\partial y^2}. \tag{2.4}$$

The suitable boundary conditions are

$$\begin{aligned} &y = 0 : u = u_w(x) = \lambda c x, \quad v = v_0, \\ &\quad N = -n\frac{\partial u}{\partial x}, \quad -\frac{\partial T}{\partial y} = h_s T \\ &y \to \infty : u \to 0, \quad N \to 0, \quad T \to T_\infty, \end{aligned} \tag{2.5}$$

where u and v are the velocity components along the x and y axes, respectively, N is the microrotation component normal to the xy-plane, κ is the vortex viscosity, j is the microinertia density, v_w is the mass transfer velocity, h is the convective heat transfer coefficient, T is the temperature of the nanofluid, h_s is the heat transfer coefficient, T_∞ is the ambient temperature and n is a constant which varies in the range $0 \le n \le 1$. The strong concentration case ($n = 0$) represents the concentrated particle flows in which the microelements close to the wall surface are unable to rotate [20]. The weak concentration case ($n = 1/2$) indicates the vanishing of the anti-symmetrical part of the stress tensor and denotes weak concentration [1]. The case $n = 1$, as suggested by Peddieson [34], is used for the modeling of turbulent boundary layer flows. $\mu_{\rm nf}$ is the viscosity of the nanofluid, $\alpha_{\rm nf}$ is the thermal diffusivity of the nanofluid and $\rho_{\rm nf}$ is the density of the nanofluid, which are given by Oztop and Abu-Nada [33].

$$\begin{aligned} \alpha_{\rm nf} &= \frac{k_{\rm nf}}{(\rho C_p)_{\rm nf}}, \quad \rho_{\rm nf} = (1-\phi)\rho_f + \phi\rho_s, \\ \mu_{\rm nf} &= \frac{\mu_f}{(1-\phi)^{2.5}}, \quad \gamma_{\rm nf} = (\mu_{\rm nf} + \kappa/2)j \\ &= \mu_f(\mu_{\rm nf}/\mu_f + K/2)j(\rho c_p)_{\rm nf} \\ &= (1-\phi)(\rho c_p)_f + \phi(\rho c_p)_s, \\ \frac{k_{\rm nf}}{k_f} &= \frac{(k_s + 2k_f) - 2\phi(k_f - k_s)}{(k_s + 2k_f) + \phi(k_f - k_s)} \\ \sigma_{\rm nf} &= \sigma_f\left[1 + \frac{3(\sigma - 1)\phi}{(\sigma + 2) - (\sigma - 1)\phi}\right], \quad \sigma = \frac{\sigma_s}{\sigma_f}. \end{aligned} \tag{2.6}$$

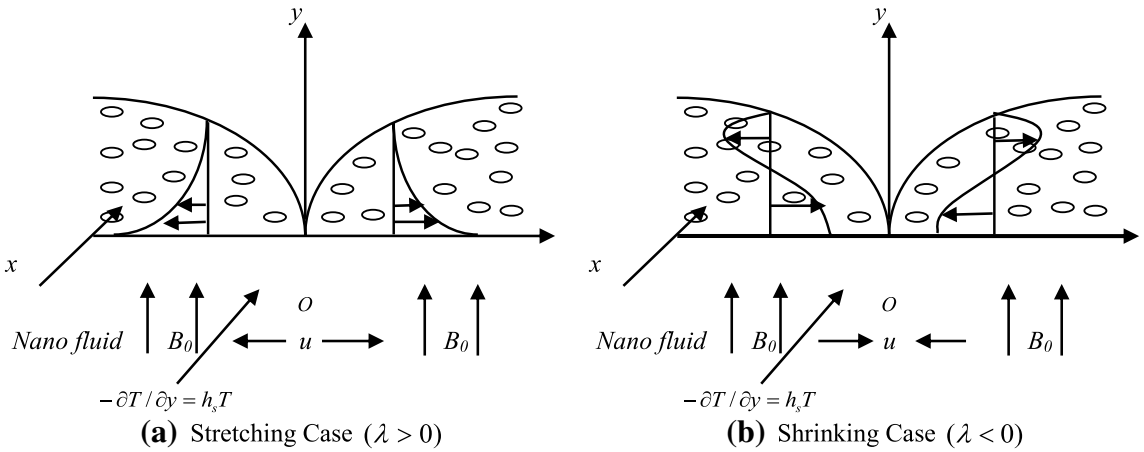

Fig. 1 Schematic diagram of the physical model

Here ϕ is the nanoparticle volume fraction, $(\rho c_p)_{nf}$ is the heat capacity of the nanofluid, δ_{nf} is the spin-gradient nanofluid viscosity, $K = \frac{\kappa}{\mu_f}$ is the micropolar or material parameter, σ_f is the electrical conductivity of the base fluid, σ_s is the electrical conductivity of the nanoparticle, k_{nf} is the thermal conductivity of the nanofluid, k_f and k_s are the thermal conductivities of the fluid and of the solid fractions, respectively, and ρ_f and ρ_s are the densities of the fluid and of the solid fractions, respectively. It should be mentioned that the use of the above expression for k_{nf} is restricted to spherical nanoparticles where it does not account for other shapes of nanoparticles [33]. Also, the viscosity of the nanofluid μ_{nf} has been approximated as viscosity of a base fluid μ_f containing dilute suspension of fine spherical particles [5].

The continuity Eq. (2.1) is satisfied by the Cauchy–Riemann equations

$$v = -\psi_x \text{ and } u = \psi_y, \tag{2.7}$$

where $\psi(x, y)$ is the stream function.

To transform the Eqs. (2.2)–(2.5) into a set of ordinary differential equations, the following similarity transformations and dimensionless variables are introduced.

$$\eta = \left(\frac{c}{\upsilon_f}\right)^{1/2} y, \quad X = (c/\upsilon_f)^{1/2} x, \quad \psi(x,y) = \upsilon_f X f(\eta)$$
$$N(x,y) = c\sqrt{c/\upsilon_f}\, x g(\eta), \quad \theta(\eta) = \frac{T - T_\infty}{T_w}, \tag{2.8}$$

where η is the similarity variable, υ_f is the kinematic viscosity of the fluid fraction and c is a constant.

After the substitution of these transformations (2.8) along with the Eq. (2.7) into the Eqs. (2.2)–(2.6), the resulting non-linear ordinary differential equations are written as

$$\frac{1 + K(1-\phi)^{2.5}}{(1-\phi)^{2.5}1 - \phi + \phi\left(\frac{\rho_s}{\rho_f}\right)} f'''(\eta) + f(\eta) f''(\eta) - f'(\eta)^2 + \frac{K}{1 - \phi + \phi\left(\frac{\rho_s}{\rho_f}\right)} g'(\eta) - M \frac{1 + \frac{3(\sigma-1)}{(\sigma+2)-(\sigma-1)\phi}}{1 - \phi + \phi\left(\frac{\rho_s}{\rho_f}\right)} f'(\eta) = 0, \tag{2.9}$$

$$\frac{1 + \frac{K}{2}(1-\phi)^{2.5}}{(1-\phi)^{2.5}1 - \phi + \phi\left(\frac{\rho_s}{\rho_f}\right)} g''(\eta) + g'(\eta) f(\eta) - f'(\eta) g(\eta) - \frac{K}{1 - \phi + \phi\left(\frac{\rho_s}{\rho_f}\right)} (2g(\eta) - f''(\eta)) = 0, \tag{2.10}$$

$$\frac{1}{\mathrm{Pr}} \frac{k_{nf}/k_f}{\left[1 - \phi + \phi(\rho C_p)_s/(\rho c_p)_f\right]} \theta''(\eta) + f(\eta)\theta'(\eta) - f'(\eta)\theta(\eta) = 0. \tag{2.11}$$

Together with the boundary conditions

$$f(0) = f_w, \quad f'(0) = \lambda, \quad g(0) = -n f''(0), \quad \theta'(0) = -\gamma(1 + \theta(0)),$$
$$f'(\eta) \to 0, \quad g(\eta) \to 0, \quad \theta(\eta) \to 0 \text{ as } \eta \to \infty. \tag{2.12}$$

Here primes denote differentiation with respect to η.

$f_w > 0$ is the suction parameter and $f_w < 0$ corresponds to injection, Pr is the Prandtl number, M is the magnetic parameter and γ is the conjugate parameter for Newtonian heating and which are given by

$$f_w = -\frac{v_0}{\sqrt{c\upsilon_f}}, \quad Pr = \frac{\mu_f (c_p)_f}{k_f}$$
$$M = \frac{\sigma_f B_0^2}{\rho_f c}, \quad \gamma = h_s \left(\frac{\upsilon_f}{c}\right)^{1/2}, \tag{2.13}$$

with $\lambda > 0$ for stretching and $\lambda < 0$ for shrinking.

The physical quantities of interest are the skin friction coefficient C_f, the couple stress C_n and the local Nusselt number Nu_x, which are defined as

$$C_f = \frac{\tau_w}{\rho u_w^2}$$
$$C_n = \frac{x}{a}\left(\frac{\partial N}{\partial y}\right)_{y=0} \tag{2.14}$$
$$Nu_x = \frac{x q_w}{k(T_\infty)},$$

where the surface shear stress τ_w and the surface heat flux q_w are given by

$$\tau_w = (\mu + \kappa)\left(\frac{\partial u}{\partial y}\right)_{y=0} + \kappa(N)_{y=0}$$
$$q_w = -k\left(\frac{\partial T}{\partial y}\right)_{y=0}, \tag{2.15}$$

with μ_{nf} and k_{nf} being the dynamic viscosity and thermal conductivity of the nanofluids, respectively.

Using the similarity variables (2.8), we obtain

$$C_f Re_x^{1/2} = (1 + (1-n)K) f''(0)$$
$$Re_x^{-1} C_n = g'(0)$$
$$\frac{Nu_x}{Re_x^{1/2}} = -\theta'(0), \tag{2.16}$$

where $Re_x = \frac{u_w x}{\upsilon}$ is the local Reynolds number.

3 Solution of the problem

The governing equations for the present problem are transformed into a set of coupled nonlinear differential

equations by applying similarity transformation. The Eqs. (2.9)–(2.11) together with the boundary conditions (2.12) are integrated numerically using Runge–Kutta–Gill method along with the shooting technique. Runge–Kutta–Gill method has the advantage of compensation for accumulated round-off error and less storage requirements than the other Runge–Kutta formulae (Kumar and Unny [23]). This method is concisely outlined as below:

$$
\begin{aligned}
&y_1 = f, \quad y_2 = f', \quad y_3 = f'', \quad y_4 = g, \quad y_5 = g', \\
&\quad y_6 = \theta, \quad y_7 = \theta' \\
&y_3' = \left[\frac{a_1 a_2}{1 + K a_1}\right]\left(y_2^2 - y_1 y_3 - \frac{K}{a_2} y_5 + M\frac{a_3}{a_2} y_2\right) \\
&y_5' = \left[\frac{a_1 a_2}{1 + \frac{K}{2} a_1}\right]\left(y_2 y_4 - y_1 y_5 + \frac{K}{a_2}(2y_4 - y_3)\right) \\
&y_7' = Pr\left[\frac{a_5}{a_4}\right](y_1 y_7 - y_2 y_6).
\end{aligned} \tag{3.1}
$$

The boundary conditions are transformed as follows:

$$
\begin{aligned}
&y_1(0) = f_w, \quad y_2(0) = \lambda, \quad y_4(0) = -n y_3(0), \\
&\quad y_7(0) = -\gamma(1 + y_6(0)) \\
&y_2(\infty) \to 0, \quad y_4(\infty) \to 0, \quad y_6(\infty) \to 0.
\end{aligned} \tag{3.2}
$$

To carry out the step by step integration for the Eqs. (2.9)–(2.12), Gill's procedures have been used (Ralston and Wilf [36]). To start the integration it is necessary to provide all the values of y_1, y_2, y_3, y_4, y_5, y_6 at $\eta = 0$ from which point, the forward integration has been carried out but from the boundary conditions it is seen that the values of y_3, y_4, y_7 are not known. So, we are to provide such values of y_3, y_4, y_7 along with the known values of the other function at $\eta = 0$ as would satisfy the boundary conditions as $\eta \to \infty$ to a prescribed accuracy after step by step integrations are performed. Since the values of y_3, y_4, y_7 which are supplied merely as rough values, some corrections have to be made in these values in order that the boundary conditions to $\eta \to \infty$ are satisfied. These corrections in the values of y_3, y_4, y_7 are taken care of by a self-iterative procedure which can for convenience be called corrective procedure.

4 Results and discussion

A numerical approach has been made out to investigate the effects of micropolar nanoparticles (Cu, Al_2O_3, TiO_2) in water-based fluid over a permeable stretching/shrinking sheet with variable suction or injection in the presence of magnetic field and Newtonian heating. To gain the physics of the problem, the velocity, angular velocity and temperature distribution profiles have been illustrated by varying controlling parameters, namely, nanoparticle volume fraction parameter (ϕ), magnetic field parameter (M), material parameter (K), stretching/shrinking parameter (λ), suction or injection parameter (f_w), Newtonian heating parameter (γ), Prandtl number (Pr), and concentration variation parameter (n). The numerical results are tabulated and exhibited with the graphical illustrations. The dual solutions (upper and lower branch solutions) are obtained for the present problem. The graphical illustrations of velocity, angular velocity and temperature distributions corresponding to dual solutions for some fixed values of governing parameters are presented in detail. From Figs. 3, 4, 5, 6, 7, 8, 9, 10, 11 and 12, it is noted that for a particular value of some parameter, there exists two different profiles with various boundary layer thicknesses, which shows the existence of dual solutions. The Prandtl number is fixed at 6.2 and the parameter n is set as 0.5.

To get a clear view of the flow field, the stream line patterns are plotted in Figs. 2 and 3 for stretching and shrinking cases. Figures 4, 5 and 6 demonstrate the influence of nanoparticles (Cu, Al_2O_3, TiO_2) on dimensionless velocity, angular velocity and temperature profiles, respectively. The other controlling parameters are set as $\phi = 0.1$, $M = 2$,

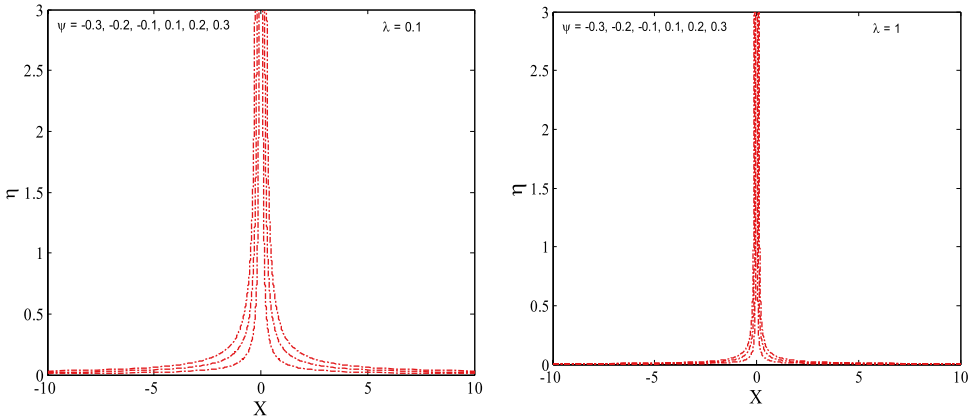

Fig. 2 Stream lines for stretching sheet when $\phi = 0.1$, $Pr = 6.2$, $M = 2$, $K = 0.3$, $f_w = 0.5$, $\gamma = 0.1$ and $n = 0.5$

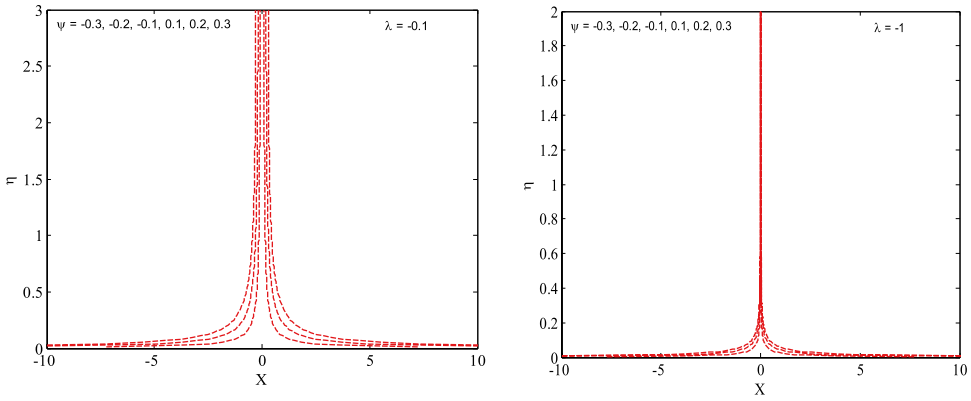

Fig. 3 Stream lines for shrinking case when $\phi = 0.1$, $Pr = 6.2$, $M = 2$, $K = 0.3$, $f_w = 0.5$, $\gamma = 0.1$ and $n = 0.5$

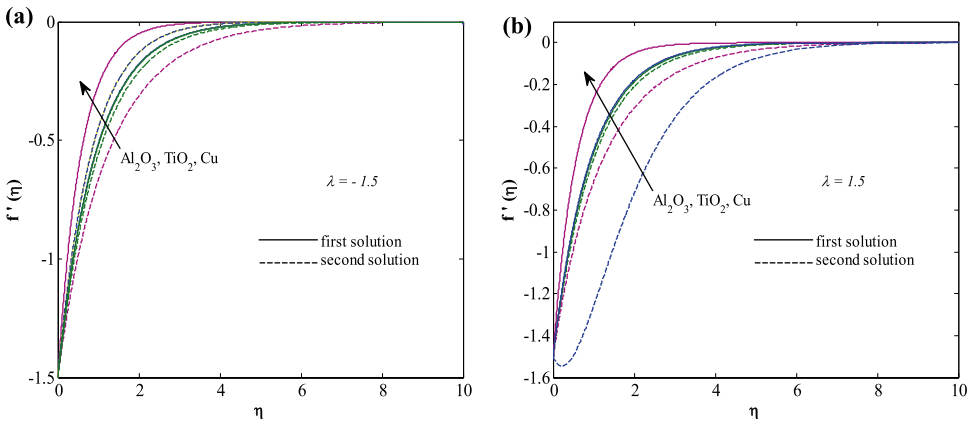

Fig. 4 Velocity profiles for different nanofluids when $\phi = 0.1$, $Pr = 6.2$, $M = 2$, $K = 0.3$, $f_w = 2.5$, $\gamma = 0.1$, $n = 0.2$ for $\lambda = -1.5$ (shrinking surface) and $\lambda = 1.5$ (stretching surface)

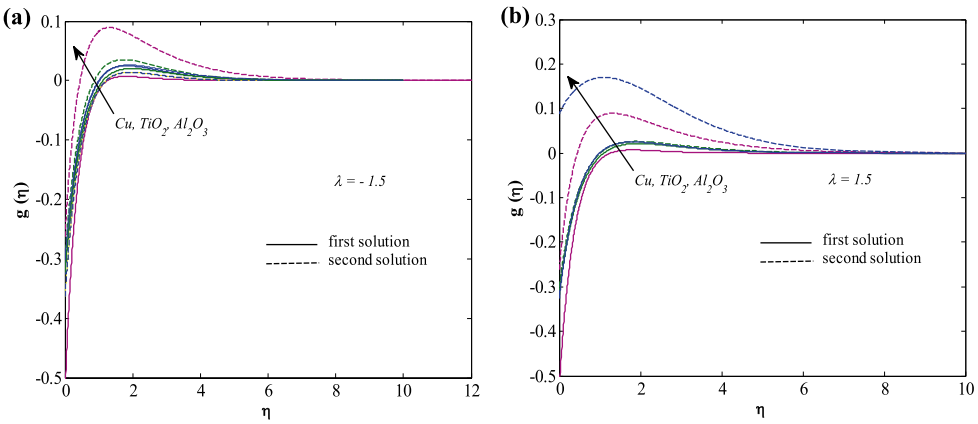

Fig. 5 Angular velocity profiles for different nanofluids when $\phi = 0.1$, $Pr = 6.2$, $M = 2$, $K = 0.3$, $f_w = 2.5$, $\gamma = 0.1$, $n = 0.5$ for $\lambda = -1.5$ (shrinking surface) and $\lambda = 1.5$ (stretching surface)

$K = 0.3$, $f_w = 2.5$ and $\gamma = 0.1$. The velocity of Cu nanofluid accelerates more than that of other nanofluids for both solutions. In the case of the second solution, it is noted that the angular velocity profile exhibits an overshoot near the shrinking sheet. Al_2O_3 nanofluid shows more angular velocity distribution than the other nanofluids under consideration. It is observed that the thickness of thermal boundary layer for Cu nanofluid is more predominant than that of other two nanofluids in the case of shrinking and stretching sheets. The physical reason behind this behavior is that Cu has the highest thermal conductivity compared to TiO_2 and Al_2O_3.

From Figs. 7, 8, 9, 10, 11, 12 and 13, the working fluid is considered as Cu–water nanofluid. The influence of suction ($f_w > 0$) parameter on velocity, angular velocity, and temperature profiles are shown in Figs. 7, 8 and 9, respectively. The other controlling parameters are fixed as $\phi = 0.1$, $M = 2$, $K = 0.3$ and $\gamma = 0.1$. For the first solution, when

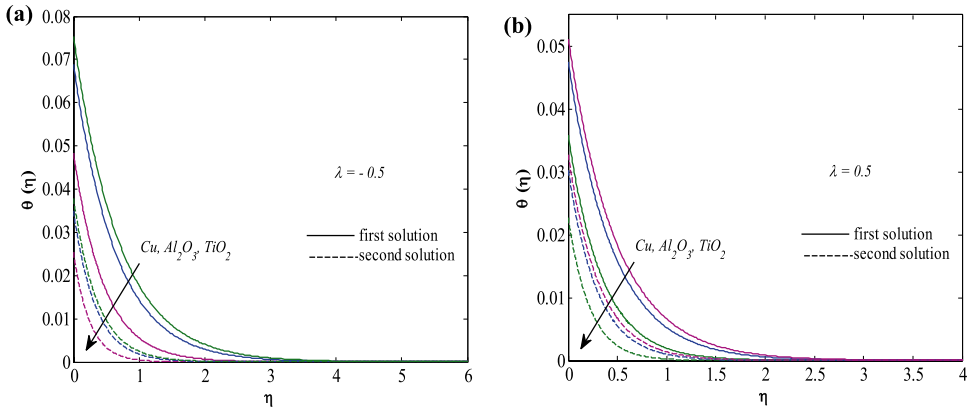

Fig. 6 Temperature profiles for different nanofluids when $\phi = 0.1$, $Pr = 6.2$, $M = 2$, $K = 0.3$, $f_w = 2.5$, $\gamma = 0.1$, $n = 0.5$ for $\lambda = -0.5$ (shrinking surface) and $\lambda = 0.5$ (stretching surface)

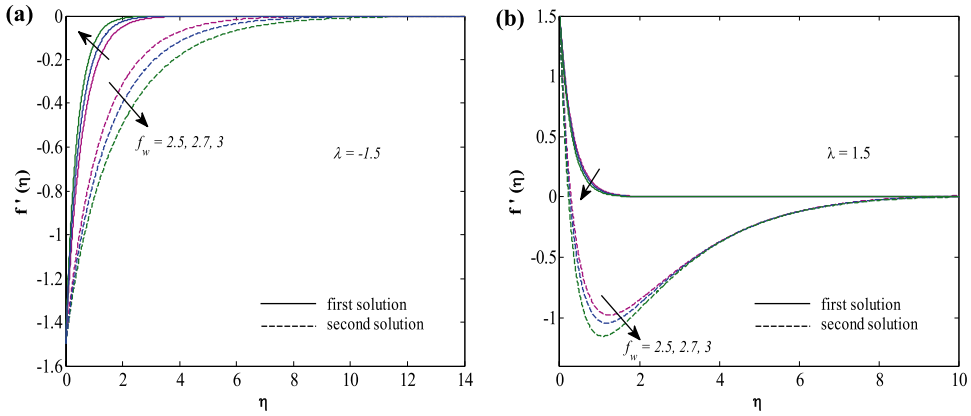

Fig. 7 Velocity profiles for f_w with Cu–water nanofluid when $\phi = 0.1$, $Pr = 6.2$, $K = 0.3$, $M = 2$, $\gamma = 0.1$, $n = 0.5$ for $\lambda = -1.5$ (shrinking surface) and $\lambda = 1.5$ (stretching surface)

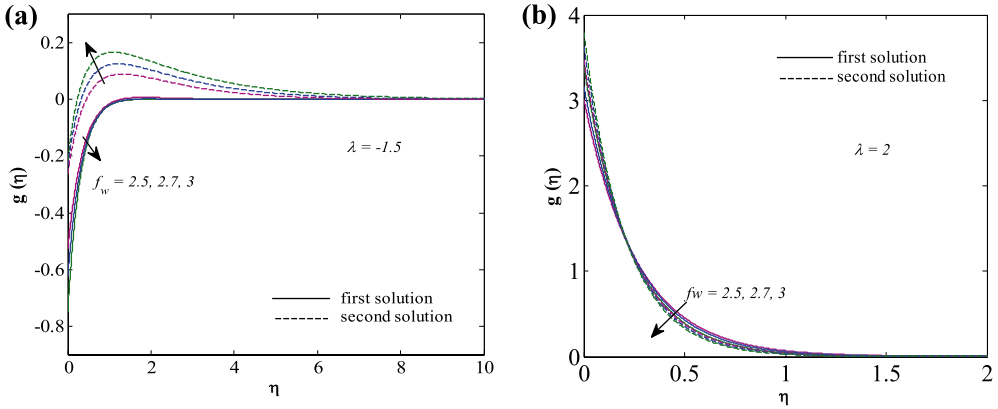

Fig. 8 Angular velocity profiles for f_w with Cu–water nanofluid when $\phi = 0.1$, $Pr = 6.2$, $K = 0.3$, $M = 2$, $\gamma = 0.1$, $n = 0.5$ for $\lambda = -1.5$ (shrinking surface) and $\lambda = 1.5$ (stretching surface)

the suction increases, the velocity and angular velocity of the fluid increases for shrinking and decrease for stretching sheets, respectively. But, the reverse results are found in the case of second solution. The thermal boundary layer thicknesses notably reduces in both solutions by increasing suction for shrinking and stretching sheets, these variations can be viewed in Fig. 9. It can be noticed that suction leads to fast cooling of the sheet and this process results in notable applications in engineering and industries.

The effect for the variation of the magnetic parameter (M) on the dimensionless velocity profile is exemplified in Fig. 10. The other parameters are assumed as $\phi = 0.1$, $K = 0.3$, $f_w = 2.5$ and $\gamma = 0.1$. It is confirmed that for the first solution, the velocity distribution is

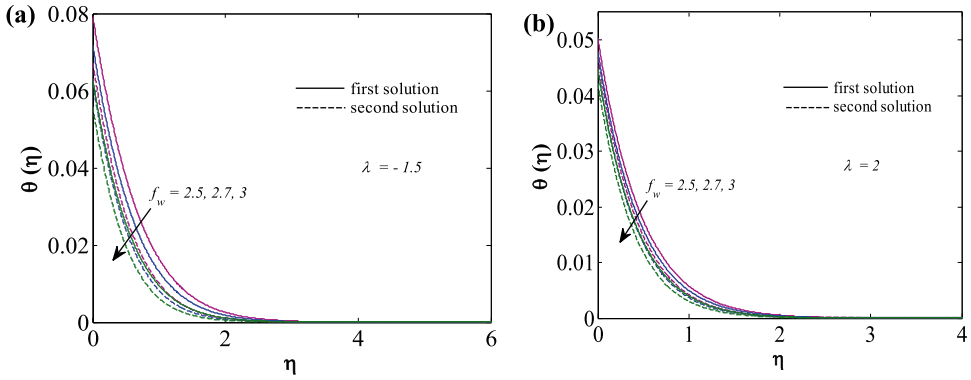

Fig. 9 Temperature profiles for f_w with Cu–water nanofluid when $\phi = 0.1$, $Pr = 6.2$, $K = 0.3$, $\gamma = 0.1$, $M = 2$, $n = 0.5$ for $\lambda = -1.5$ (shrinking surface) and $\lambda = 2.0$ (stretching surface)

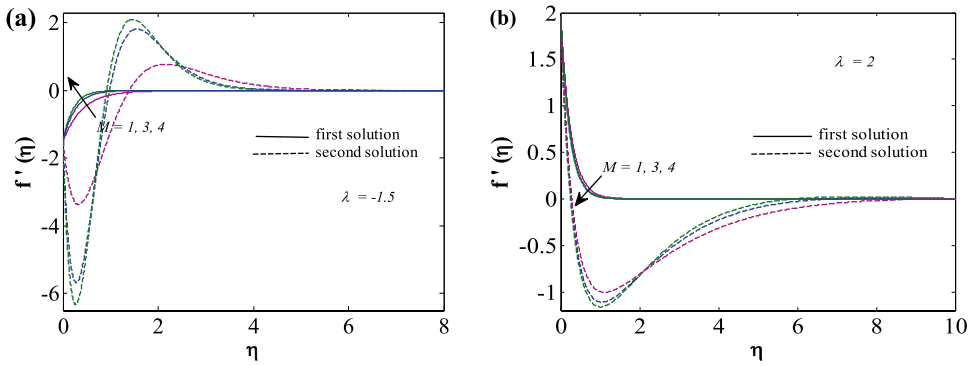

Fig. 10 Velocity profiles for M with Cu–water nanofluid when $\phi = 0.1$, $Pr = 6.2$, $K = 0.3$, $f_w = 2.5$, $\gamma = 0.1$, $n = 0.5$ for $\lambda = -1.5$ (shrinking surface) and $\lambda = 2.0$ (stretching surface)

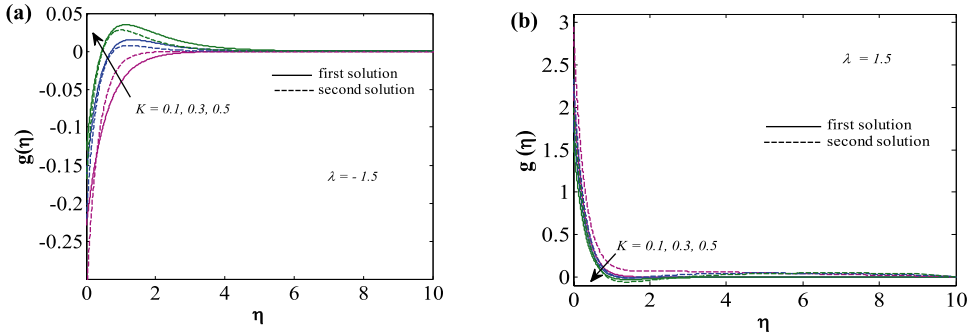

Fig. 11 Angular velocity profiles for K with Cu–water nanofluid when $\phi = 0.1$, $Pr = 6.2$, $M = 2$, $f_w = 2.5$, $\gamma = 0.1$, $n = 0.5$ for $\lambda = -1.5$ (shrinking surface) and $\lambda = 1.5$ (stretching surface)

significantly increased near the shrinking sheet while the value of magnetic parameter is increased. An increase in the magnetic parameter leads to a stronger Lorentz force. Stronger Lorentz force creates resistance in the fluid flows that appears in the reduction of velocities. As far as the second solution is considered magnetic field remarkable affects the velocity profile for both sheets.

The influence of material parameter (K) on dimensionless velocity, angular velocity and temperature profiles is presented in Fig. 11. The discussion is carried out for the constant values of the other parameters such as $\phi = 0.1$, $M = 2$, $f_w = 2.5$ and $\gamma = 0.1$. As a result, it can be observed that the angular velocity strictly increases considerably when material parameter increases for shrinking sheet. Furthermore, opposite results are observed for stretching sheet.

The effects of solid volume fraction of nanoparticles (ϕ) on the dimensionless temperature profile are exemplified in Fig. 12a, b. The effects of solid volume fraction (ϕ) are described by assuming the values of other parameters as $M = 2$, $K = 0.3$, $f_w = 2.5$ and $\gamma = 0.1$. It is noticed that for both solutions, as solid volume fraction parameter increases, the thermal boundary layer thickness increases for shrinking and stretching sheets.

The effects of Newtonian heating (γ) parameter on the dimensionless temperature profile are depicted in Fig. 13. The other controlling parameters are set as $\phi = 0.1$, $M = 2$, $K = 0.3$ and $f_w = 2.5$. When conjugate

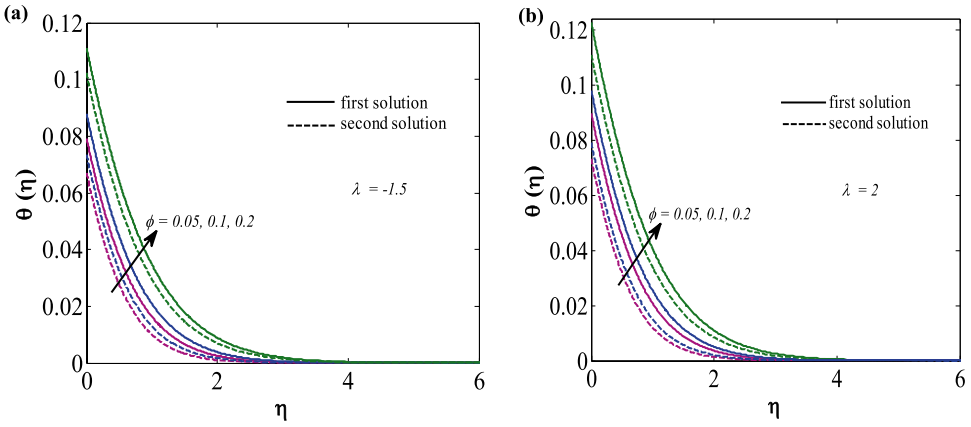

Fig. 12 Temperature profiles for ϕ with Cu–water nanofluid when $Pr = 6.2$, $M = 2$, $f_w = 2.5$, $n = 0.5$, $\gamma = 0.1$, $K = 0.3$ for $\lambda = -1.5$ (shrinking surface) and $\lambda = 2.0$ (stretching surface)

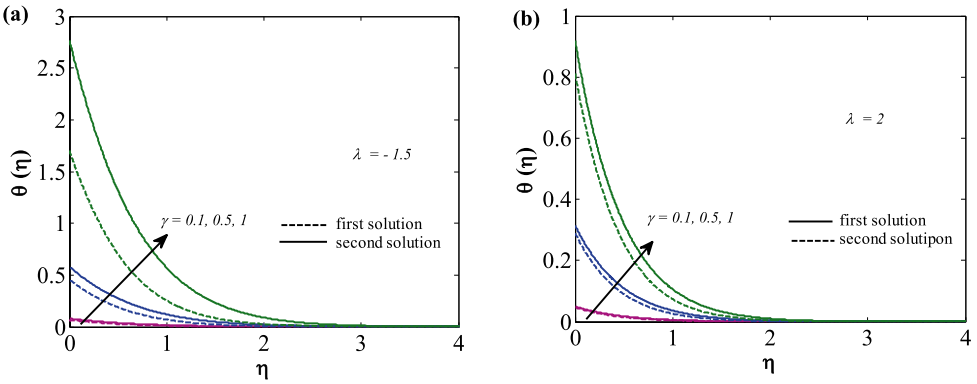

Fig. 13 Temperature profiles for γ with Cu–water nanofluid when $\phi = 0.1$, $\mathrm{Pr} = 6.2$, $M = 2$, $K = 0.3$, $f_w = 2.5$, $n = 0.5$ for $\lambda = -1.5$ (shrinking surface) and $\lambda = 2.0$ (stretching surface)

Table 2 Comparison of $Re_x^{1/2} C_f$ for K and n when $\lambda = 1$, $\phi = 0$ and $f_w = 0$

K	$Re_x^{1/2} C_f$					
	$n = 0$			$n = 0.5$		
	Present study	Fauzi et al. [15]	Nazar et al. [30]	Present study	Fauzi et al. [15]	Nazar et al. [30]
0	−1.000008	−1.00000	−1.0000	−1.000008	−1.0000	−1.0000
1	−1.367996	−1.3680	−1.3679	−1.224820	−1.2248	−1.2247
2	−1.621575	−1.6225	−1.6213	−1.414479	−1.4159	−1.4142
4	−2.005420	−2.0075	−2.0042	−1.733292	−1.7381	−1.7321

parameter for Newtonian heating (γ) increases, thicknesses of the thermal boundary layer considerably increase for both surfaces. In fact, the conjugate parameter for Newtonian heating effect not only has the tendency to increase the fluid temperature but also increases the thermal boundary layer thickness of sheets sizeably.

Dual solutions are classified as first solution and second solution. Weidman et al. [43], Rosca and Pop [40], Nazar et al. [31], Merkin [26], and Sharma et al. [41] are examined stability analysis to determine which solution is stable and physically applicable. They are proved that the first solution is the stable solution and second one is unstable. Moreover, it is worth mentioning that both solutions satisfied the far field boundary conditions asymptotically, which are supporting the validity of the obtained numerical results. To verify the accuracy of our present results, comparisons have been made with the available results of Fauzi et al. [15] and Nazar et al. [30] in the literature, which are shown in Tables 2, 3, 4, 5, 6, 7 and 8. In Table 2, comparison of the local skin friction ($Re_x^{1/2} C_f$) for stretching case and viscous fluid in the absence of suction or injection is presented. Tables 3, 4 and 5 illustrate the comparison results of skin friction coefficient for Cu, Al_2O_3 and TiO_2 in water-based micropolar nanofluids, respectively. Tables 6, 7 and 8 shows the comparison results of couple

Table 3 Comparison of $\mathrm{Re}_x^{1/2}C_f$ for f_w when $\lambda = 1, K = 2, n = 0.5, Pr = M = \gamma = 0$ for Cu

f_w	$Re_x^{1/2}C_f$					
	$\phi = 0.05$		$\phi = 0.1$		$\phi = 0.2$	
	Present study	Fauzi et al. [15]	Present study	Fauzi et al. [15]	Present study	Fauzi et al. [15]
0	−1.617787	−1.6258	−1.766825	−1.7726	−1.942730	−1.9466
1	−2.399188	−2.4026	−2.711805	−2.7136	−3.103236	−3.1041
2	−3.389040	−3.3896	−3.918142	−3.9183	−4.595383	−4.5954
2.5	−3.935964	−3.9362	−4.582944	−4.5830	−5.414644	−5.4147
3	−4.506066	−4.5061	−5.274059	−5.2741	−6.263688	−6.2637

Table 4 Comparison of $Re_x^{1/2}C_f$ for f_w when $\lambda = 1, K = 2, n = 0.5, Pr = M = \gamma = 0$ for Al_2O_3

f_w	$Re_x^{1/2}C_f$					
	$\phi = 0.05$		$\phi = 0.1$		$\phi = 0.2$	
	Present study	Fauzi et al. [15]	Present study	Fauzi et al. [15]	Present study	Fauzi et al. [15]
0	−1.466842	−1.4779	−1.502291	−1.5125	−1.524793	−1.5344
1	−2.099890	−2.1059	−2.168640	−2.1738	−2.212781	−2.2175
2	−2.894216	−2.8959	−3.006760	−3.0081	−3.079371	−3.0805
2.5	−3.333942	−3.3347	−3.470558	−3.4711	−3.558798	−3.5592
3	−3.793529	−3.7938	−3.955007	−3.9552	−4.059377	−4.0595

Table 5 Comparison of $Re_x^{1/2}C_f$ for f_w when $\lambda = 1, K = 2, n = 0.5, Pr = M = \gamma = 0$ for TiO_2

f_w	$Re_x^{1/2}C_f$					
	$\phi = 0.05$		$\phi = 0.1$		$\phi = 0.2$	
	Present study	Fauzi et al. [15]	Present study	Fauzi et al. [15]	Present study	Fauzi et al. [15]
0	−1.475768	−1.4867	−1.518439	−1.5283	−1.551364	−1.5604
1	−2.117111	−2.1229	−2.200267	−2.2052	−2.265378	−2.2696
2	−2.922341	−2.9239	−3.058766	−3.0599	−3.166265	−3.1642
2.5	−3.368064	−3.3687	−3.533754	−3.5342	−3.664503	−3.6649
3	−3.833847	−3.8341	−4.029750	−4.0299	−4.184476	−4.1846

Table 6 Comparison of $Re_x^{-1}C_n$ for f_w when $\lambda = 1, K = 2, n = 0.5, Pr = M = \gamma = 0$ for Cu

f_w	$Re_x^{-1}C_n$					
	$\phi = 0.05$		$\phi = 0.1$		$\phi = 0.2$	
	Present study	Fauzi et al. [15]	Present study	Fauzi et al. [15]	Present study	Fauzi et al. [15]
0	−0.327110	−0.3273	−0.390814	−0.3903	−0.471763	−0.4719
1	−0.719509	−0.7201	−0.919235	−0.9196	−1.203758	−1.2040
2	−1.435699	−1.4359	−1.918979	−1.9191	−2.639693	−2.6397
2.5	−1.936476	−1.9366	−2.625422	−2.6255	−3.664796	−3.6648
3	−2.538079	−2.5381	−3.476963	−3.4770	−4.904224	−4.9042

stress ($Re_x^{-1}C_n$) for various nanofluids under investigation. It is established that the results obtained in the present work demonstrate a good agreement with the previously published results.

5 Conclusions

In the present paper, the steady, two dimensional flow of micropolar nanofluids with heat transfer over permeable

Table 7 Comparison of $Re_x^{-1}C_n$ of f_w when $\lambda = 1, K = 2, n = 0.5, Pr = M = \gamma = 0$ for Al_2O_3

f_w	$Re_x^{-1}C_n$					
	$\phi = 0.05$		$\phi = 0.1$		$\phi = 0.2$	
	Present study	Fauzi et al. [15]	Present study	Fauzi et al. [15]	Present study	Fauzi et al. [15]
0	−0.268876	−0.2691	−0.282042	−0.2823	−0.290563	−0.2903
1	−0.551181	−0.5521	−0.587866	−1.0869	−0.612038	−0.6129
2	−1.047061	−1.0475	−1.130075	−1.1305	−1.185313	−1.1857
2.5	−1.389396	−1.3897	−1.505597	−1.5058	−1.583130	−1.5833
3	−1.798858	−1.7989	−1.955260	−1.9554	−2.059818	−2.0599

Table 8 Comparison of $Re_x^{-1}C_n$ for f_w when $\lambda = 1, K = 2, n = 0.5, Pr = M = \gamma = 0$ for TiO_2

f_w	$Re_x^{-1}C_n$					
	$\phi = 0.05$		$\phi = 0.1$		$\phi = 0.2$	
	Present study	Fauzi et al. [15]	Present study	Fauzi et al. [15]	Present study	Fauzi et al. [15]
0	−0.272161	−0.2724	−0.288143	−0.2883	−0.300786	−0.3010
1	−0.560259	−0.5611	−0.605139	−0.6059	−0.641482	−0.6422
2	−1.067509	−1.0679	−1.169506	−1.1699	−1.253152	−1.2535
2.5	−1.417982	−1.4182	−1.560927	−1.5611	−1.678572	−1.6787
3	−1.837298	−1.8374	−2.029861	−2.0299	−2.188730	−2.1888

stretching/shrinking sheet with variable suction/injection in the presence of magnetic field and Newtonian heating is investigated. The governing equations are approximated to a system of non-linear ordinary differential equations by similarity transformation. Numerical calculations are carried out for various values of the dimensionless parameters of the problem. The results also show the existence of dual solutions for both stretching and shrinking cases. The drawn conclusions for the present work after a thorough observation are summarized as follows:

1. Dual solutions are found for some values of the governing parameters for both stretching and shrinking sheets.
2. The thermal boundary layer thicknesses notably reduce by increasing suction parameter for shrinking sheet.
3. On increasing material parameter, the angular velocity of the fluid significantly increases near the shrinking sheet.
4. For both solutions, when the solid volume fraction parameter is increased, an increase in the thermal boundary layer thickness is found for the sheets under consideration.

Acknowledgements The authors gratefully acknowledge the reviewers for their constructive comments and valuable suggestions.

References

1. Ahmadi G (1976) Self-similar solution of incompressible micropolar boundary layer flow over a semi-infinite plate. Int J Eng Sci 14:639–646
2. Arafa AA, Gorla RSR (1992) Mixed convection boundary layer flow of a micropolar fluid along vertical cylinders and needles. Int J Eng Sci 30:1745–1751
3. Baag S, Mishra SR (2015) Heat and mass transfer analysis on MHD 3-D water-based nanofluid. J Nanofluids 4:1–10
4. Bourantas GC, Loukopoulos VC (2014) MHD natural convection flow in a inclined square enclosure filled with a micropolar nanofluid. Int J Heat Mass Transf 29:930–944
5. Brinkman HC (1952) The viscosity of concentrated suspensions and solutions. J Chem Phys 20:571
6. Buongiorno J (2006) Convective transport in nanofluids. ASME J Heat Transf 128:240–250
7. Chaudhary RC, Jain P (2007) An exact solution to the unsteady free convection boundary layer flow past an impulsively started vertical surface with Newtonian heating. J Eng Phys Thermophys 80:954–960
8. Choi SU (1995) Enhancing thermal conductivity of fluids with nanoparticles. ASME Publ Fed 231:99–106
9. Choi SUS, Zhang ZG, Yu W, Lockwood FE, Grulke EA (2001) Anomalous thermal conductivity enhancement in nanotube suspensions. Appl Phys Lett 79:2252–2254
10. Cramer KR, Pai SI (1973) Magnetofluid dynamics for engineers and applied physicists. McGraw-Hill, New York
11. Das S, Jana RN (2015) Natural convective magneto-nanofluid flow and radiative heat transfer past a moving vertical plate. Alex Eng J 54:55–64
12. El-Dabe NT, Ghaly AY, Rizkallah RR, Ewis KM, Al-Bareda AS (2015) Numerical solution of MHD boundary layer flow of non-Newtonian Casson fluid on a moving wedge with heat and

mass transfer and induced magnetic field. J Appl Math Phys 3:649–663
13. Erignen AC (1966) Theory of micropolar fluids. J Math Mech 16:1–18
14. Erignen AC (1972) Theory of thermomicrofluids. J Math Appl 38:480–496
15. Fauzi ELA, Ahmad S, Pop I (2014) Flow over a permeable stretching sheet in micropolar nanofluids with suction. In: Proceedings of the 21st national symposium on mathematical sciences (SKSM21): Germination of Mathematical Sciences Education and Research towards Global Sustainability 1605: 428–433
16. Gireesha BJ, Gorla RSR, Mahanthesh B (2015) Effect of suspended nanoparticles on three-dimensional MHD flow, heat and mass transfer of radiating Eyring–Powell fluid over a stretching sheet. J Nanofluids 4:1–11
17. Hayat T, Awais M, Asghar S (2013) Radiative effects in a three-dimensional flow of MHD Eyring–Powell fluid. J Egypt Math Soc 21:379–384
18. Hayat T, Nawaz M (2010) Magnetohydrodynamic three-dimensional flow of a second-grade fluid with heat transfer. Z Naturforsch 65:683–691
19. Jat RN, Jhankal AK (2003) Three-dimensional free convective MHD flow and heat transfer through a porous medium. Indian J Eng Mater Sci 10:138–142
20. Jena SK, Mathur MN (1981) Similarity solutions for laminar free convection flow of a thermomicropolar fluid past a non-isothermal vertical flat plate. Int J Eng Sci 19:1431–1439
21. Kar M, Dash GC, Sahoo SN, Rath PK (2013) Three-dimensional free convection MHD flow in a vertical channel through a porous medium with heat source and chemical reaction. J Eng Thermodyn 22:203–215
22. Khan A, Khan I, Shafie S (2016) Effects of Newtonian heating and mass diffusion on MHD free convection flow over vertical plate with shear stress at the wall. J Teknol 78:71–75
23. Kumar A, Unny TE (1977) Application of Runge–Kutta method for the solution of non-linear partial differential equations. Appl Math Model 1(4):199–204
24. Makinde OD, Aziz A (2011) Boundary layer flow of a nanofluid past a stretching sheet with a convective boundary condition. Int J Therm Sci 50:1326–1332
25. Makinde OD, Mishra SR (2015) On stagnation point flow of variable viscosity nanofluids past a stretching surface with radiative heat. Int J Appl Comput Math 1:1–18
26. Merkin JH (1985) On dual solutions occurring in mixed convection in a porous medium. J Eng Math 20(2):171–179
27. Merkin JH (1994) Natural convection boundary layer flow on a vertical surface with Newtonian heating. Int J Heat Fluid Flow 15:392–398
28. Mohamed MKA, Salleh MZ, Nazar R, Ishak A (2012) Stagnation point flow over a stretching sheet with Newtonian heating. Sains Malays 41:1467–1473
29. Nadeem S, Rehman A, Vajravelu K, Lee J, Lee C (2012) Axisymmetric stagnation flow of a micropolar nanofluid in a moving cylinder. Math Probl Eng 2012:1–18
30. Nazar R, Ishak A, Pop I (2008) Unsteady boundary layer flow over a stretching sheet in a micropolar fluid. Int J Math Phys Eng Sci 2:161–165
31. Nazar R, Noor A, Jafar K, Pop I (2014) Stability analysis of three-dimensional flow and heat transfer over a permeable shrinking surface in a Cu–water nanofluid. Int J Math Comput Phys Electr Comput Eng 8:776–782
32. Noor NFM, Haq RU, Nadeem S, Hashim I (2015) Mixed convection stagnation point flow of a micropolar nanofluid along a vertically stretching surface with slip effects. Mechanica 50:2007–2022
33. Oztop HF, Abu-Nada E (2008) Numerical study of natural convection in partially heated rectangular enclosures filled with nanofluids. Int J Heat Fluid Flow 29:1326–1336
34. Peddieson J (1972) An application of the micropolar fluid model to the calculation of a turbulent shear flow. Int J Eng Sci 10:23–32
35. Rajagopal K, Veena PH, Pravin VK (2013) Unsteady three-dimensional MHD flow due to impulsive motion with heat and mass transfer past a stretching sheet in a saturated porous medium. Int J Appl Mech Eng 18:137–151
36. Ralston A, Wilf HS (Eds.) (1976) Mathematical methods for digital computers (Vol. 1). John Wiley & Sons
37. Ram Reddy C, Pradeepa T, Srinivasacharya D (2015) Similarity solution for free convection flow of a micropolar fluid under convective boundary condition via lie scaling group transformations. Adv High Energy Phys 2015:1–16
38. Ramzan M (2015) Influence of Newtonian heating on three-dimensional MHD flow of couple stress nanofluid with viscous dissipation and joule heating. PLoS One 10(4):e0124699
39. Rehman A, Nadeem S (2012) Mixed convection heat transfer in micropolar nanofluid over a vertical slender cylinder. Chin Phys Lett 29:124701
40. Rosca AV, Pop I (2013) Flow and heat transfer over a vertical permeable stretching/shrinking sheet with a second order slip. Int J Heat Mass Transf 60(1):355–364
41. Sharma R, Ishak A, Pop I (2014) Stability analysis of magnetohydrodynamic stagnation-point flow toward a stretching/shrinking sheet. Comput Fluids 102:94–98
42. Turkyilmazoglu M (2012) Three dimensional MHD stagnation flow due to a stretchable rotating disk. Int J Heat Mass Transf 55:6959–6965
43. Weidman PD, Kubitschek DG, Davis AMJ (2006) The effect of transpiration on self-similar boundary layer flow over moving surfaces. Int J Eng Sci 44(11–12):730–737